Subcritical thermoacoustic bifurcation in turbulent combustors: effects of inertia

Giacomo Bonciolini[1,*], Dominik Ebi[2], Edouard Boujo[1] and Nicolas Noiray[1]
[1]CAPS Laboratory, MAVT department, ETH Zürich, Zurich, Switzerland
[2]Laboratory for Thermal Processes and Combustion, Paul Scherrer Institute, Villigen, Switzerland

1 Introduction

Thermoacoustic coupling is a recurring issue in many combustion systems, such as gas turbine combustors or rocket engines [1]. This phenomenon is due to a constructive interaction between heat release rate fluctuations and acoustic pressure oscillations. In fig. 1 one can see the resulting average cycle that the flame undergoes when the combustor investigated in this study is operated at a linearly unstable condition. When such a limit cycle is triggered in a real engine, the corresponding high acoustic levels can be detrimental for its mechanical integrity, which might prevent the user to operate it at its maximum performance point. The thermoacoustic stability depends on the operating condition at which the machine is run, e.g. on inlet temperature, pressure, air/fuel ratio and so on. In some cases, the system can experience a subcritical bifurcation when one of these parameters is varied, switching suddenly from a stable operation to a high-amplitude limit cycle. In the following section, experimental data obtained from a lab-scale, fully pre-mixed, atmospheric combustor showing this phenomenon will be presented.

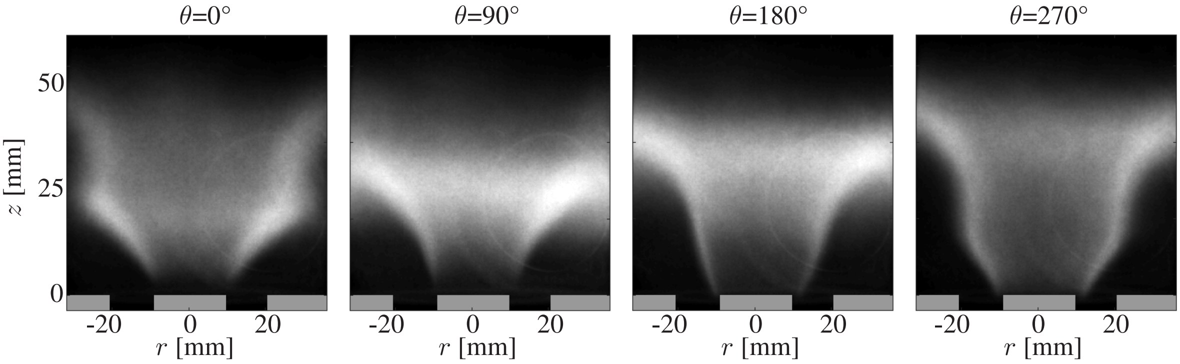

Figure 1: Lab-scale combustor flame phase-averaged OH^* chemiluminescence intensity at four different phase angles.

*Correspondence to: giacomob@ethz.ch

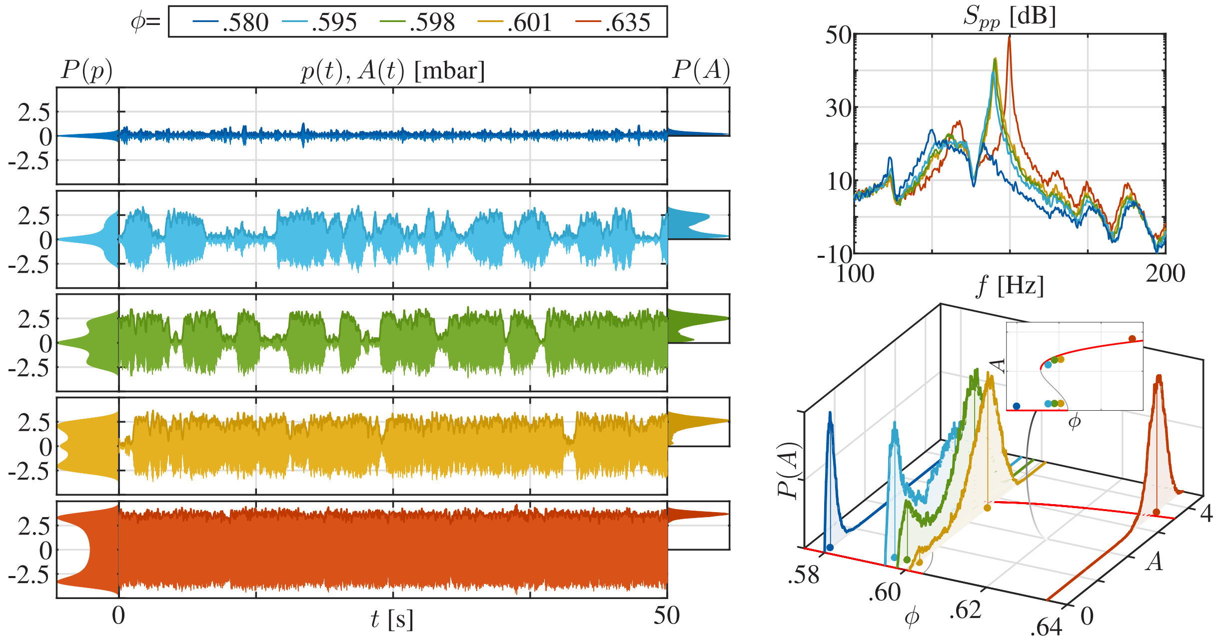

Figure 2: Left: combustor dynamic pressure $p(t)$ (light) and amplitude $A(t)$ (dark) signals and corresponding statistics at five different operating points. Top right: corresponding power spectral density S_{pp}. Bottom right: detail of the amplitude PDFs with the underlying subcritical bifurcation.

1.1 Stationary experiments

Figure 2 presents time traces of acoustic pressure $p(t)$ (light) and amplitude $A(t)$ (dark), and their corresponding statistics acquired at different equivalence ratio ϕ of the air/methane mixture. From top to bottom, i.e. for increasing ϕ, a subcritical Hopf bifurcation can be observed. For low ϕ the system is linearly stable, with only small amplitude acoustics caused by turbulence-induced heat release rate fluctuations. Then, for intermediate ϕ, the combustor is bistable, presenting two high probability states (see $P(A)$) alternatively visited by the system. The switch between these two states is, again, driven by the background turbulence forcing, and a mean transition time from one to the other can be computed. This time changes along the bistable region, together with $P(A)$: in the three central rows, when the high-amplitude state becomes more frequent (for increasing ϕ), the time that the system stays in the low-amplitude range before transitioning to the high-amplitude one becomes shorter. When ϕ is further increased, the system leaves the bistable region of the bifurcation diagram and has, as the only equilibrium point, a high-amplitude limit cycle. One can observe how the onset of the limit cycle corresponds to a change of the pressure power spectrum, with a sharp peak at the frequency of the limit cycle oscillation becoming predominant. In the bottom right of fig. 2, the five amplitude Probability Density Functions (PDF) and their local maxima are compared to a deterministic bifurcation diagram obtained from a simple model of the system dynamics. A very good agreement is found. Details about the model are provided in the next section.

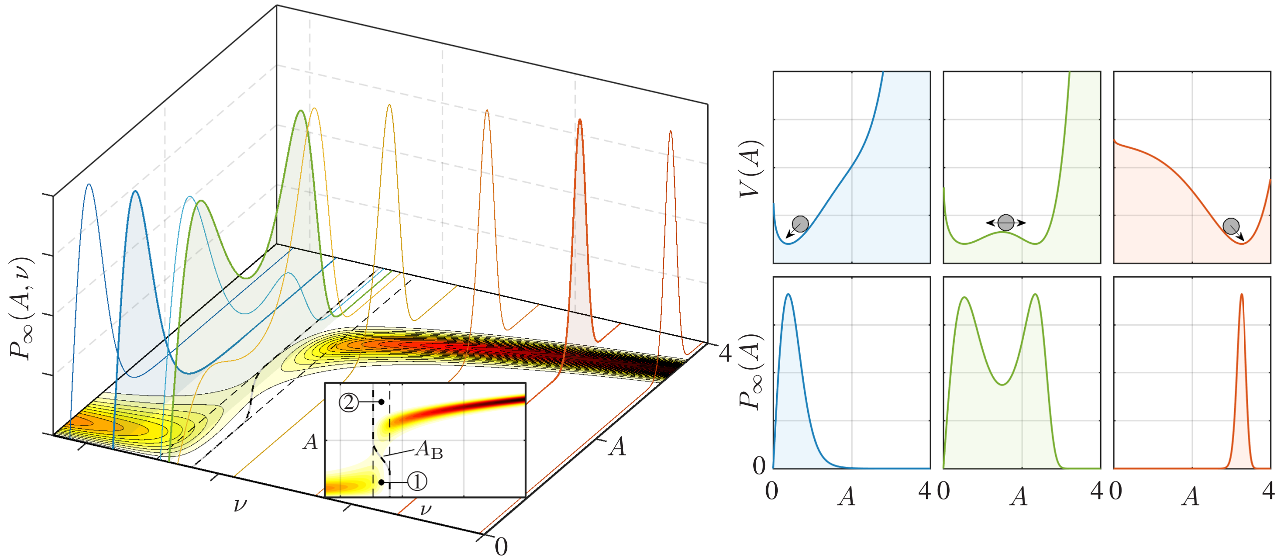

Figure 3: Stationary Amplitude PDF of the oscillator model. Left: stationary PDF as a function of the control parameter ν. In the inset, the same PDF, with the bistable region highlighted with two potential wells (① and ②) separated by the potential barrier $A_\mathrm{B}(\nu)$. Right: detail of three selected points (linearly stable, bistable, linearly unstable), with their potential $V(A)$ and stationary PDF $P_\infty(A)$.

1.2 Low-order model of the system

A simple model of a thermoacoustic system with subcritical bifurcation is given by the nonlinear oscillator:

$$\ddot{p} + \omega_0^2 p = [2\nu + \kappa p^2 - \gamma p^4]\dot{p} + \xi, \tag{1}$$

where ω_0 is the angular frequency, ν the oscillation linear growth rate, κ and γ two positive constants that define the non-linear response of the oscillator. The term ξ is a white noise forcing of intensity Γ that models non-coherent turbulence-induced heat release rate fluctuations. Following the derivation in [2], one can assume $p(t) = A(t)\cos(\omega_0 t + \phi(t))$, derive a Langevin equation for the slowly-varying amplitude $A(t)$ and the associated Fokker-Planck equation (FPE) for the variation in time of the Amplitude PDF $P(A,t)$:

$$\frac{\partial}{\partial t}P(A,t) = -\frac{\partial}{\partial A}[\mathcal{F}(A)P(A,t)] + \frac{\Gamma}{4\omega_0^2}\frac{\partial^2}{\partial A^2}P(A,t), \tag{2}$$

where $\mathcal{F}(A) = A\left(\nu + \frac{\kappa}{8}A^2 - \frac{\gamma}{16}A^4\right) + \frac{\Gamma}{4\omega_0^2 A} = -\mathrm{d}V/\mathrm{d}A$, i.e. the derivative of a potential. Setting $\partial P/\partial t = 0$, one obtains the stationary PDF $P_\infty(A,\nu)$, plotted in fig. 3 in a bifurcation diagram fashion, as a function of the linear growth rate ν. One can observe the bistability region, bounded between the two dotted lines. This corresponds to the range of ν that generates a potential $V(A)$ featuring two minima, i.e. two potential wells separated by a potential barrier at $A = A_\mathrm{B}(\nu)$.

2 Ramping of the control parameter

To highlight the peculiar transient dynamics of the system, the bifurcation parameter has been varied over time. Experimental results are presented, and then compared to the low-order model (1) simulations.

2.1 Experimental ramping of the equivalence ratio ϕ

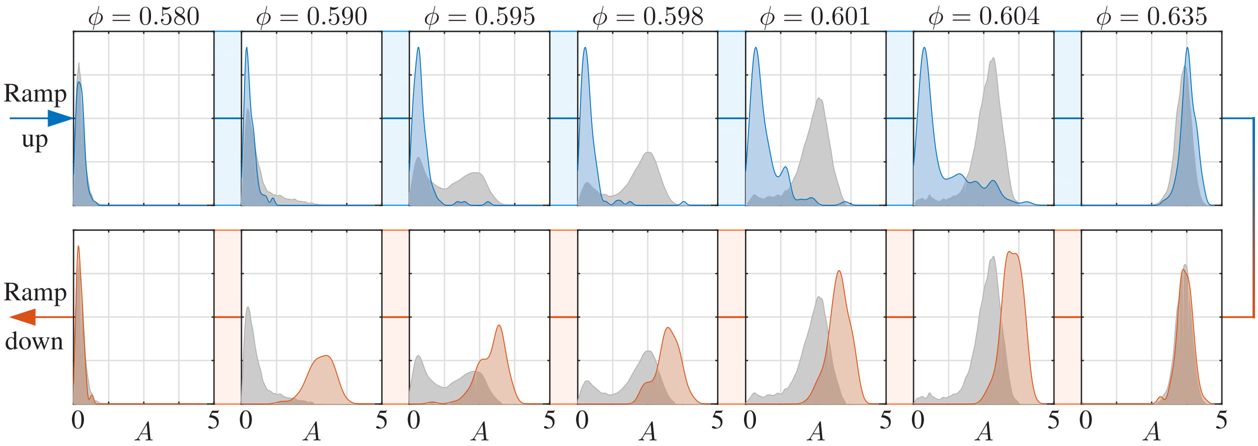

Figure 4: Comparison of the stationary probability density function $P(A)$ at seven equivalence ratios ϕ (grey) and the evolution in time of the PDF when ϕ is ramped up (top row, blue) and down (bottom row, red).

In this experiment, the fuel mass flow controller is regulated via an ad-hoc designed signal. The resulting combustible mixture has an equivalence ratio increasing linearly in 4s in the range $\phi = 0.580 \rightarrow 0.635$, then idling for 10s at the maximum, ramping back to the minimum ϕ in 4s and finally staying at this equivalence ratio for another 10s. This cycle is repeated 100 times. In fig. 4 the statistics of this experiment are presented. The 14 panels are grouped in two rows, the top one corresponds to the 100 ramps up, the bottom one to the 100 ramps down. Each column corresponds to an equivalence ratio. The PDFs of the ramp experiment, obtained via a kernel density estimation applied to the 100 realisations, are plotted in color (blue for the ramp up, red for the ramp down). In each panel the stationary Amplitude PDF at the corresponding ϕ (grey shading) is given as a reference. One can observe the hysteresis experienced by the system: in the bistable region, even if the stationary PDF features two maxima, the system stays in the low-amplitude (high-amplitude) range, when ϕ is ramped up (down). Another feature is the delay in transition, easily observable in the bottom row: the dynamic PDF peak is at higher amplitude compared to the one of the stationary PDF at the same ϕ. This means that the system experiences inertial effects, remaining longer close to the initial state. This effect is governed by the ramp speed, and it will be investigated in details making use of the system model.

2.2 Model ramping of the linear growth rate ν

A single oscillator is a valid surrogate of a real system in the present case, as the examined mode is isolated from the others. If more modes were present, a network of oscillators would be required: ramping can trigger switching between neighbouring modes. Time domain simulation of eq. (1) and numerical solution of eq. (2) are performed with ν varying linearly in a time t_{ramp}. The two approaches are in very good agreement, as exemplified in fig. 5a-b. Other solutions of the FPE are presented in fig. 5c-f, where the ramp up and down are compared at two additional ramp speeds. One can first observe how the hysteresis is correctly captured. Then, a delay in the transition from the quiet regime to the loud one (and vice-versa) is observed: the oscillations remain bounded for some time in a range of small (high) amplitudes even though,

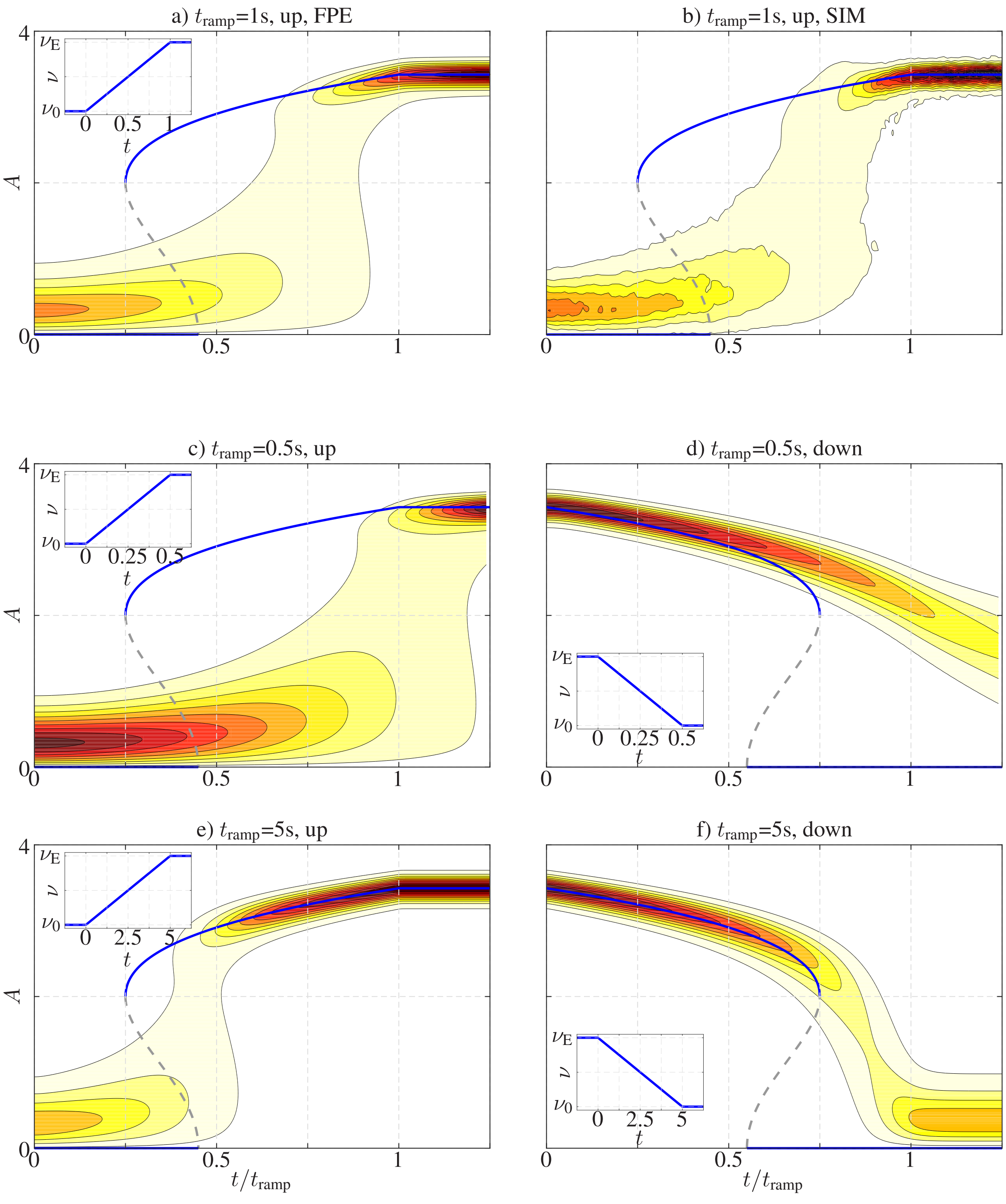

Figure 5: Comparison between numerical solution of the FPE (a) and time domain simulation (b) for a ramp of ν in t_{ramp}=1s. (c-f) Solution of the FPE at two additional ramp speeds (rows), and two ramp directions (columns): from linearly stable to limit cycle regime (left), and vice-versa (right).

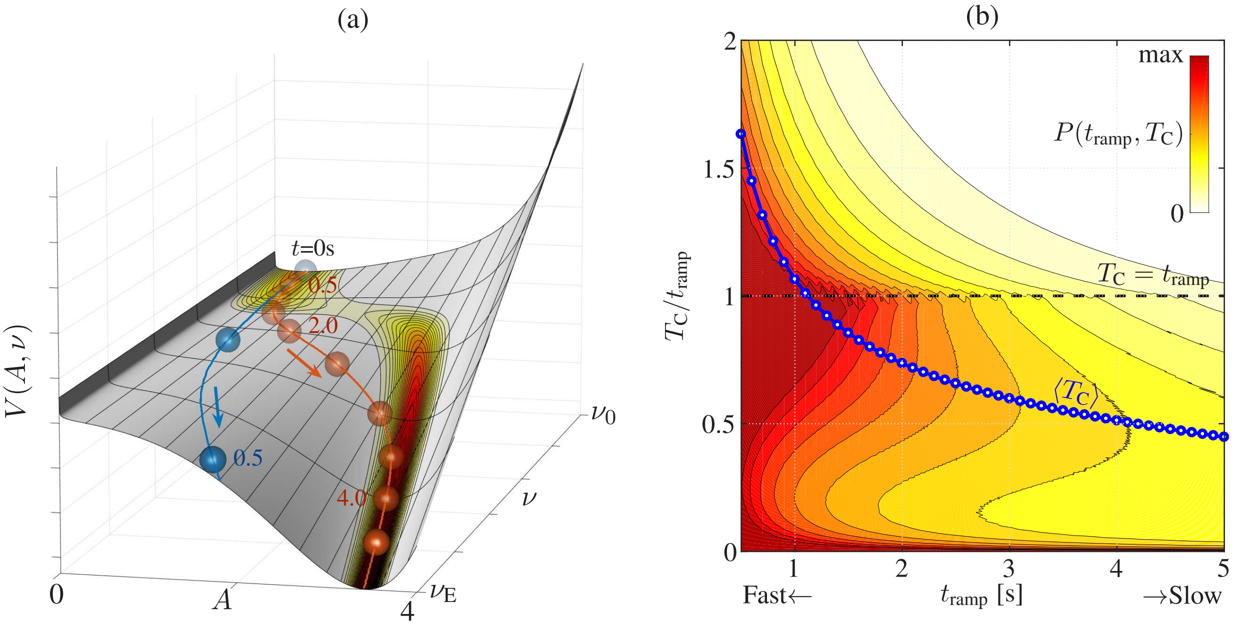

Figure 6: a) Mechanical analogy of the process, described as a ball rolling on the potential surface $V(A,\nu)$: ball mean path for two ramping times $t_{ramp} = 0.5$s (blue) and $t_{ramp} = 5$s (red). b) Relative first crossing time T_C/t_{ramp} statistic, as a function of the ramp time t_{ramp}. In blue, the mean crossing time $\langle T_C(t_{ramp})\rangle$.

in the stationary case, these points would be unstable. The ν at which the transition finally occurs is less delayed, in terms of ν, when t_{ramp} is longer. In fig. 6a this phenomenon is presented via a mechanical analogy: the state is represented by a ball rolling on the potential surface $V(A,\nu)$. When the ball is "fast" (blue), its inertia makes it roll straighter than the "slow" (red) ball, which falls in the high-amplitude well right after the latter appears. To quantify the time needed to transit from the low to the high-amplitude oscillation regime during the ramping, the statistic of the time T_C needed to cross the moving potential barrier $A_B(\nu(t))$ was computed. This was done both by performing many simulations of the process and by solving the FPE with a moving absorbing boundary condition imposed on $A_B(t)$. Figure 6b shows the results of the FPE method as a function of the ramp time t_{ramp}. The inertial effects have a stronger relevance for fast ramping, leading to a longer T_C/t_{ramp}. This translates into a higher value of ν at the moment of transition and therefore to a higher amplitude of the suddenly triggered limit cycle. This fact has a practical relevance in real combustion systems such as gas turbines: we conclude demonstrating that a control system designed to protect the machine from unexpected pressure rise would be less effective if the operating point is varied too quickly.

References

[1] Poinsot T. (2016), Prediction and control of combustion instabilities in real engines, *Proceedings of the Combustion Institute*.

[2] Noiray, N. (2016), Linear growth rate estimation from dynamics and statistics of acoustic signal envelope in turbulent combustors, *Journal of Engineering for Gas Turbines and Power 139.4: 041503*.